Journal of Loss Prevention in the Process Industries 76 (2022) 104739

Contents lists available at ScienceDirect

Journal of Loss Prevention in the Process Industries

journal homepage: www.elsevier.com/locate/jlp

Comparison of thermal runaway pressures within sealed enclosures for nickel manganese cobalt and iron phosphate cathode lithium-ion cells

Thomas H. Dubaniewicz *, Teresa L. Barone, Connor B. Brown, Richard A. Thomas

National Institute for Occupational Safety and Health (NIOSH), 626 Cochrans Mill Road, Pittsburgh, PA, 15236, United States

ARTICLE INFO

Keywords:
Lithium-ion battery thermal runaway
Explosion-proof enclosures
Flame-proof enclosures
Vented explosions

ABSTRACT

Mining vehicle manufacturers are developing lithium-ion (Li-ion) battery electric vehicles as an alternative to diesel-powered vehicles. In gassy underground mines, explosion-proof (XP) enclosures are commonly used to enclose electrical ignition sources to prevent propagation of an internal methane-air explosion to a surrounding explosive atmosphere. Li-ion batteries can create pressurized explosions within sealed enclosures due to thermal runaway (TR). NIOSH researchers measured TR pressures of nickel manganese cobalt (NMC) cathode type 18650 Li-ion cells, model MH1, as a function of free space within sealed enclosures and observed an inverse power relationship. TR pressure-rise rates, gas quantities, and temperatures were also measured. A confined NMC cell with 92.5 mL of free space produced 232 bar of pressure, far exceeding minimum pressure containment specifications for conventional XP enclosures. Approximately 287 times the cell volume of free space would be needed to reduce the TR pressure of these cells to 8.62 barg (125 psig) per U.S. Code of Federal Regulations, Title 30, Part 18. The NMC cell TR pressures were significantly higher than those measured previously for iron phosphate cathode Li-ion cells under comparable confinement conditions.

1. Introduction

Battery electric vehicle (BEV) development for underground mining continues at a rapid pace (Leonida, 2021). From a diesel emissions reduction perspective, the benefits of employing BEVs are arguably greater for underground mining than any other industry (GMG, 2018). Approximately 15,000 underground coal miners and 13,000 underground metal/nonmetal miners in the USA are exposed to aerosols and gases emitted by diesel engines, and exposure of underground miners to diesel aerosols is the highest among workers in all occupations (NIOSH, 2020). Given the relatively high energy density of Li-ion batteries, they are currently the most common battery of choice for new BEV applications (GMG, 2018). Large-format batteries of hundreds of volts sourcing hundreds of amperes are constructed from series and parallel connections of smaller cells or modules. The difficult operating conditions within the mine environment poses challenges for large-battery management systems (Kurpiel et al., 2021). With proper design and maintenance, mishaps involving Li-ion battery thermal runaway (TR) leading to fire or explosion should be rare. However, several mishaps have occurred in underground mines in the early stages of BEV deployment (Gillett, 2021; Jacques, 2019), emphasizing the ongoing need to mitigate fire and explosion hazards.

Researchers at the National Institute for Occupational Safety and Health (NIOSH), Pittsburgh Mining Research Division (PMRD), are studying approaches to mitigate the fire and explosion hazards of Li-ion batteries used for mining equipment. The potential use of Li-ion BEVs in gassy underground mines poses unique explosion hazards. Dubaniewicz et al. (Dubaniewicz and DuCarme, 2016; Dubaniewicz et al., 2021) reviewed the gassy mine explosion hazard and the use of explosion-proof (XP) or flame-proof enclosures for explosion protection of electrical equipment. XP or flame-proof enclosures are commonly used in potentially explosive atmospheres in mines to enclose electrical ignition sources to prevent propagation of an internal methane (CH_4)/air explosion to a surrounding CH_4 and coal dust contaminated atmosphere. The U.S. Mine Safety and Health Administration (MSHA) develops and enforces safety and health rules for all U.S. mines. According to MSHA design requirements (U.S. Code of Federal regulation, 2021), XP enclosures must withstand a minimum pressure of at least 150 psig (10.3 barg) and the external surfaces of enclosures shall not exceed 150 °C (302 °F). For required explosion testing (MSHA, 2005), if any pressure peak exceeds 125 psig (8.62 barg), the manufacturer must either make constructional changes that will result in a reduction of

* Corresponding author.
E-mail address: tcd5@cdc.gov (T.H. Dubaniewicz).

https://doi.org/10.1016/j.jlp.2022.104739
Received 13 December 2021; Received in revised form 19 January 2022; Accepted 22 January 2022
Available online 24 January 2022
0950-4230/Published by Elsevier Ltd.

pressure to 125 psig or less or conduct static pressure tests of the enclosure, with the enclosure withstanding a static pressure of twice the highest value recorded in any previous tests. These MSHA requirements pertain to ignition of CH_4-air. There are no established test procedures for assessing pressures from Li-ion battery TR.

Dubaniewicz et al. (2021) characterized TR pressures of lithium iron phosphate (LFP) cathode cells as a function of enclosure free space. A well-confined LFP cell with 3 mL of free space produced 294 bar (4260 psia) of pressure during a TR, far exceeding pressure containment specifications for conventional XP enclosures. Using a curve fit equation, they estimated that approximately 34 times the LFP cell volume of free space would be needed to meet the 125-psig pressure generation threshold under the specified test conditions. Results of the work support a safety alert for flame-proof enclosures that the explosion energy generated when cells fail can far exceed the mechanical strength of the enclosure and would therefore not prevent the ignition propagating to the open atmosphere (Pyroban, 2021). In the current work, NIOSH researchers characterized TR pressures of nickel manganese cobalt (NMC) cathode Li-ion cells in a similar fashion. NMC is one of several Li-ion cathode chemistries used for mining BEVs (GMG, 2018; Jacques, 2019). Enclosure-confined cells were heated in an accelerating rate calorimeter (ARC) to attain TR, simulating excessive temperatures within XP enclosures due to potential internal CH_4-air ignition, electrical fault within a large-format battery, or fault within Li-ion cells susceptible to TR from internal short circuit.

A wide range of maximum TR pressures have been reported for NMC cathode Li-ion batteries. Duh et al. (2021) reviewed TR characteristics of commercial Li-ion batteries used in electric vehicles and found TR pressures for NMC cells ranging from 5.9 to 38.3 bar (Jhu et al., 2012; Yayathi et al., 2016; Duh et al., 2017; Zhao et al., 2020). The 38.3-bar result was obtained within a 400-mL vessel (Duh et al., 2017). Duh et al. (2021) noted that "Maximum pressure and pressure-rising rate are not taken account of consideration because of the significant dependence on volume of the test system." Yuan et al. (2020) reported a TR pressure above 100 bar for a test using an NMC cell within a sealed canister with an internal volume of 220 cm^3. The current work employed a range of sealed enclosure volumes to better characterize maximum TR pressure and pressure time rate (dP/dt) as a function of enclosure free space.

The gas liberated by the ruptured Li-ion cell during TR as well as its characteristic temperature rise is responsible for the pressure developed in the containment vessel for well-confined cells (Dubaniewicz et al., 2021). Gully et al. (2019) observed that off-gassing of the LFP and NMC cells studied produced 2–9.2 L/Ah of vent gas. They also observed that an NMC cell TR that did not induce visible combustion external to the cell released significantly more gas than others that did induce visible combustion. The difference was attributed to consumption of vent gas by combustion external to the cell. Gully et al. (2019) indicated that the total gas production volume tends to be proportional to the Ah size of the battery that is involved in the off-gas scenario. Several other researchers have reported on TR gas generation in terms of gas volume per Ah as well (Koch et al., 2018; Hoelle et al., 2021). It should be noted that similar cells connected in series provide the same Ah capacity as that of a single cell. Therefore, the total estimated amount of gas potentially released by a large-format battery with series-connected cells may be underestimated if the Ah rating of the large-format battery is used. The energy (e.g. Wh) factors in both voltage and current capacity of a large-format battery with series connected cells. The use of energy rather than current capacity may avoid confusion when scaling up gas production from a failing cell to ratings for a large-format battery.

Deflagration vents are used to vent the combustion gases and pressures resulting from a deflagration within an enclosure to minimize structural and mechanical damage (NFPA, 2018). McKinnon et al. (2020) identified the lack of deflagration venting per NFPA 68 (2018) as a contributing factor to a battery energy storage system thermal runaway and explosion event that seriously injured several responders. Hill (2020) indicates that some energy storage system integrators and designers have opted for the use of deflagration panels.

Much of the literature on Li-ion battery explosion venting pertains to the ignition of flammable gas-air mixtures that may form from battery off-gassing (Gully et al., 2019; Zalosh et al., 2021; Baird et al., 2020; Henriksen et al., 2019; Stephens et al., 2017). Flammability characteristics of vented gas-air mixtures are used for deflagration vent design per standards such as NFPA 68. However, application of NFPA 68 to a Li-ion battery enclosure may be problematic if TR is taken into consideration. The standard does not apply to emergency vents for pressure generated during runaway exothermic reactions, self-decomposition reactions, internal vapor generation resulting from electrical faults, or pressure generation mechanisms other than deflagration (NFPA, 2018). Most if not all of these exclusions appear to apply to Li-ion battery TR. Regarding maximum pressure, well-confined Li-ion batteries can produce TR pressures exceeding vent gas-air ignition pressures by well over an order of magnitude (Dubaniewicz et al., 2021). Also, TR vent gas flow may be supersonic and turbulent (Mishra et al., 2021). TR characteristics of Li-ion batteries should be taken into consideration for the design of such enclosure vents.

Pressure-relieving vents are often integrated into the casing of cylindrical Li-ion cells. Cell vents are intended to relieve pressure build-up within the cell and to dissipate heat in an attempt to prevent TR; however, the vents are not always effective (Yao et al., 2020). Finegan et al. (2018) explain that a rapid rise in pressure can circumvent the safety mechanisms of even the most advanced cell designs. Improperly designed or obstructed cell vents can lead to the release of projectiles or side-wall ruptures that may damage or enhance the heating of adjacent cells, potentially leading to a cascading TR throughout a large battery.

NIOSH researchers and a battery electric vehicle (BEV) manufacturer established a testing agreement to conduct a TR pressure test of a 100-Ah NMC cathode Li-ion pouch cell housed within a sealed enclosure. The objective of the test was to see if a confined cell produced a TR pressure that exceeded the 8.62-barg (125-psig) pressure generation threshold specification for conventional MSHA-approved XP enclosures. The cooperating BEV manufacturer provided the NMC pouch cell and a rugged form-fitting enclosure. NIOSH researchers conducted the TR test and recorded the data. The test extends the format and capacity of NMC Li-ion cells under study.

2. Material and methods

2.1. Li-ion cells

Three different types of cells were used for the ARC tests. Type 18650 NMC 811 cathode cells, model MH1, were used for measurements of TR pressures as a function of free space. The cell provided by the BEV manufacturer was a 100-Ah NMC pouch cell. The NMC ratio of the pouch cell was not disclosed. An LFP type 26650 cell was used for one ARC test with pressures measured at the same sampling rate as the MH1 cells. The LFP cell was the same make and model studied previously (Dubaniewicz et al., 2021). The cells were conditioned with three charge-discharge cycles followed by a charge to 100% state of charge. A multichannel potentiostat/galvanostat (MSTAT, Arbin Instruments, College Station, Texas) cycled the cells using cell-manufacturer-specified parameters. Discharge capacities for the MH1 and LFP cells were at least 95% of rated capacity using C/2 charge and discharge rates. The discharge capacity of the pouch cell was 105 Ah

Table 1
Electrical ratings for Li-ion cells.

Cell	Type	Capacity (Ah)	Voltage (V)	Energy (Wh)
NMC 811 (MH1)	18650	3.2	3.67	11.7
LFP	26650	3.8	3.2	12.2
NMC	pouch	100	3.68	368

using C/20 charge and discharge rates. Electrical ratings for the cells are listed in Table 1. Cell energy was calculated from the rated voltage and current capacity.

The MH1 cell was characterized to confirm the cathode composition specified by the manufacturer and to evaluate other components, including the anode and separator. The components were characterized by scanning electron microscopy (SEM; Model S-4800, Hitachi, Tokyo, Japan) and energy dispersive x-ray spectroscopy (EDS; Bruker Quantax, Madison, Wisconsin). The samples for SEM/EDS analysis were extracted from the MH1 cell after fully discharging it for personnel safety and were mounted on 25-mm aluminum posts with conductive carbon tape. The separator was coated with gold and palladium to avoid image distortion from a lack of sample conductivity, while the anode and cathode remained uncoated due to their high conductivity. The analysis of the cathode showed that the ratio of nickel to manganese and cobalt approached 8:1:1, which is a composition known for its high specific capacity. However, this composition has a shorter life cycle and lower thermal abuse tolerance than another common ratio of 5:2:3 (Nitta et al., 2015). The analysis of the anode indicated that it contained the common active material, graphite. The graphite particles of the anode had relatively large sizes and uniform morphology, which can enhance battery tolerance of thermal abuse (Park and Lee, 2009; Adams et al., 2019). The anode spectra also showed weak peaks for fluorine and phosphorous, which suggests that it contained a small amount of lithium salt from the electrolyte solution (e.g., lithium hexafluorophosphate) (Harris et al., 2009; Campion et al., 2004). The separator was composed of a porous ceramic membrane of alumina or lithium aluminate along with an organic coating or membrane. This composite separator has a more resistant structure than one with an organic membrane only (Nestler et al., 2014; Raja et al., 2015). Overall, the characterization suggested that the cathode had a composition with a relatively low thermal abuse tolerance but was balanced by a robust anode and separator.

2.2. Experimental setup

Researchers used an ARC system (model EV+, Thermal Hazard Technology, Milton Keynes, United Kingdom) and an independent data acquisition system (model DI-720, DATAQ Instruments, Akron, Ohio) for TR pressure measurements. The Li-ion cell was sealed within a cylindrical canister (for the MH1 and LFP cells) or steel plate enclosure (for the pouch cell) and placed within the ARC (Figs. 1–2). Three MH1 cells were placed within a canister for one test. The ARC temperature was raised to a constant value to provide steady-state heating until the cell reached TR. The heaters shut off after TR detection. ARC instrumentation included voltage inputs and type N thermocouples (0.81-mm diameter) which were used for most tests. Voltage and temperature were not measured for tests using the smallest canisters due to space limitations and high pressures that caused the thermocouple fittings to fail. An ARC enhanced system (ARCes) control and data acquisition software recorded voltage and temperature data. The data was imported into Microsoft Excel for analysis. The ARC video camera was used for the 100-Ah pouch cell ARC test to monitor for venting from a pressure relief valve attached to the cell enclosure.

Several pressure sensors were available ranging from 21 bar (300 psia) to 689 bar (sealed) (10,000 psis) maximum pressure. The pressure sensor used for a particular ARC test was selected based on the anticipated peak TR pressure. The pressure sensor was connected to the canister or enclosure using short lengths of tubing. The internal tubing volume was factored into sealed enclosure internal volume estimates. The tubing outside diameter was at least 1/8 inch (3.175 mm). A DATAQ Instruments model DI-720 data acquisition system recorded pressures at 100 samples per second, consistent with MSHA test procedures for explosion testing (MSHA, 2005). The pressure sensor data was imported into Microsoft Excel for analysis.

Various sizes of canisters provided different amounts of free space around the MH1 cells (Fig. 1). The canisters were constructed in-house from steel pipe nipples with caps screwed onto both ends. Their internal volumes were measured by filling them with water. The larger canisters are schedule 40, and the smaller canisters are schedule 80. The caps were drilled and tapped to accept compression fittings for instrumentation.

Fig. 1. Canisters provided varying amounts of free space around enclosed Li-ion cells.

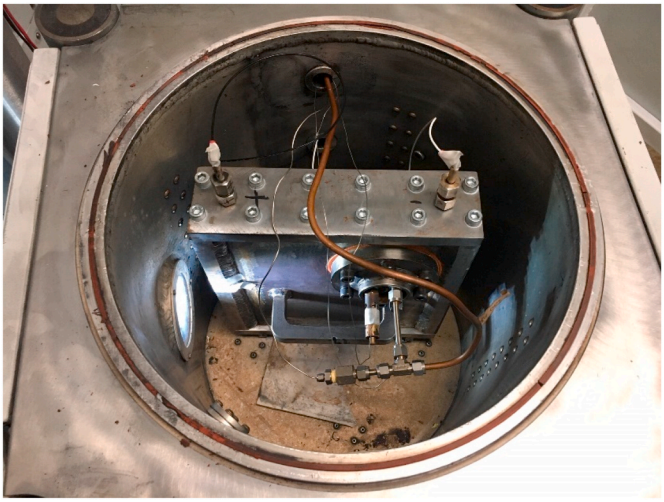

Fig. 2. The steel plate enclosure housing the NMC pouch cell placed within the ARC.

The enclosure for the 100-Ah NMC pouch cell test was fabricated by the BEV manufacturer from 1-inch-thick (2.54 cm) steel plate. Rubber gaskets sealed the bolted enclosure joints. Holes were drilled and tapped in the enclosure to accept compression fittings and a pressure relief valve. The pressure relief valve was used for safety purposes. It had a set pressure of 20.7 barg (300 psig) and a rated flow of 8495 L/min. Fig. 2 shows the enclosure placed within the EV + ARC. Pliable tubing connected this heavy enclosure to a pressure sensor located outside of the EV + ARC. The internal volume of the tubing was approximately 8 mL. The enclosure provided a tight fit around the pouch cell with very little free space.

3. Results

3.1. Pressures

Fig. 3 shows DATAQ recorded pressures for an 18650 MH1 and a 26650 LFP cell within similar canisters. Free space was 685 mL and 667 mL for the MH1 and LFP cell, respectively. The larger size of the LFP cell reduced the free space slightly. A small increase in pressure occurred during cell venting followed by a larger increase during TR. The MH1 cell produced a sharp pressure peak during TR, whereas the pressure response of the LFP cell was more gradual. The LFP cell took significantly longer to reach TR due to its higher exothermic onset temperature (Dubaniewicz et al., 2021) and larger mass (88 versus 45 mg). The MH1 cell produced a much higher peak pressure than the LFP cell even though their electrical energies are similar (Table 1). Fig. 4 shows a time plot of dP/dt for this MH1 cell at TR. The negative pressure rate after TR may indicate condensation of less volatile gas species (Dubaniewicz et al., 2021).

Fig. 5 shows the pressure time plot for the three-cell test with 1215 mL of free space. Three distinct pressure rises and a pressure additive effect are apparent as the cells went into TR in quick succession.

Table 2 lists maximum TR pressures, maximum pressure rise time rates $(dP/dt)_{max}$, and deflagration index values (K_{MH1}) for the MH1 cells sealed within various canisters. NFPA 68 (2018) defines the deflagration index K as

$$K = (dp/dt)_{max} V^{1/3}$$

where $(dP/dt)_{max}$ is the maximum rate of pressure rise attained by combustion in a closed vessel with volume V. The free spaces listed in Table 2 are the estimated volume within the canister plus connected tubing minus the nominal volume (16.54 mL) of the type 18650 MH1 cell. Pressure values are absolute. The last entry in Table 2 is for a test with three cells inside of a canister. Figs. 6–8 show an inverse power relationship with free space/cell volume for maximum TR pressure, maximum pressure rise rate, and deflagration index. The three-cell-test result is near the trend curves of the single-cell tests for the normalized confinement conditions (Free space/cell vol.). Figs. 6–8 illustrate how small void space volumes may be problematic in terms of safety hazards associated with TR overpressures and rates of pressure rise.

3.2. Temperatures

Fig. 9 shows time plots of temperature and cell voltage for a representative single-cell ARC test, in this case, an MH1 cell with 685 mL free space inside of the canister. The cell thermocouple was taped to the metallic surface of the cell about mid-length with fiber tape. The gas thermocouple was inserted into free space within the canister, and the canister thermocouple was taped to the canister exterior. Cell heating from internal exothermic processes, including chemical reactions and internal short circuit, increased after venting as the cell temperature crossed over to exceed the canister exterior surface temperature. Internal short circuit is indicated by voltage dropout. Peak cell and gas temperatures resulted from external heating and heating from cell internal exothermic processes. Temperature summary data are shown as box and whisker plots in Figs. 10 and 11. The temperature at venting onset is the temperature at which initial venting became apparent from dP/dt data. The difference between peak and venting onset temperatures provides an approximation of temperature rise due to cell exothermic processes including TR.

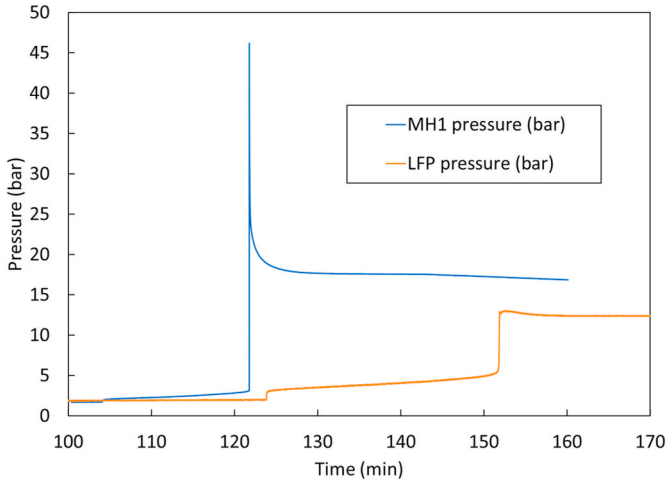

Fig. 3. TR pressure time plots of MH1 and LFP cells with similar energies tested within similar canisters.

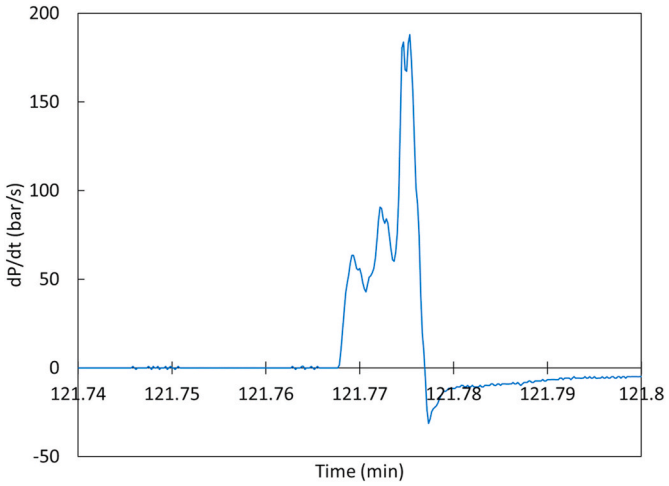

Fig. 4. Time plot of dP/dt for an MH1 cell at TR with 685 mL of free space.

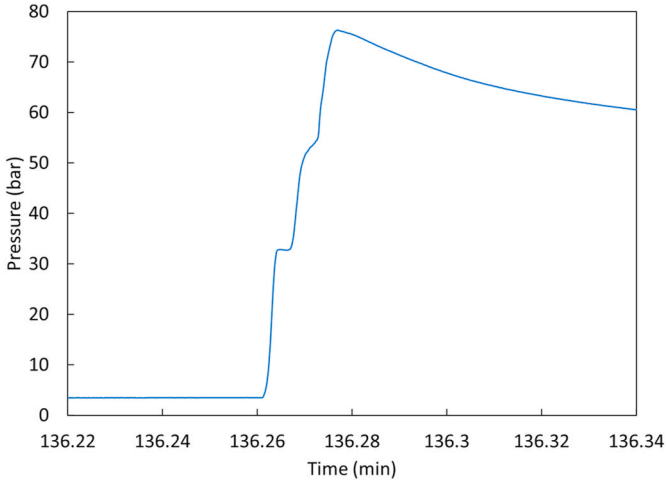

Fig. 5. Additive pressure effect of three MH1 cell thermal runaways in quick succession (1215 mL of free space).

3.3. Quantity of gas

The pressure and temperature for a given canister were used to calculate the moles of gas produced by the MH1 cells per the ideal gas law. The moles of gas were then used to convert the gas volume to ambient temperature and pressure conditions (22 °C and 1.0 bar). Fig. 12 shows representative time traces of pressure, gas temperature, and the converted ambient volume of vent and TR gases for an MH1 ARC

Table 2
Thermal runaway (TR) maximum pressures, maximum pressure rise rates, and deflagration indices for MH1 cells within sealed canisters.

Free space (mL)	Free space/cell volume	Pressure (bar)	dP/dt (bar/s)	K_{MH1} (m·bar/s)
92.5	5.6	192	1450	65.4
92.5	5.6	231	2000	90.6
92.5	5.6	231	2530	115
168	10.2	161	1730	95.7
168	10.2	140	1170	64.3
168	10.2	165	1610	88.9
267	16.2	76.5	366	23.6
267	16.2	70.9	459	29.6
267	16.2	110	704	45.4
685	41.4	43.4	337	30.2
685	41.4	46.1	172	15.4
685	41.4	46.2	188	16.8
1278	77.3	24.7	138	15
1278	77.3	24.1	185	20.1
1278	77.3	25.9	182	19.8
2393	145	15.4	110	14.7
2393	145	14.9	103	13.8
2393	145	14.3	83.5	11.2
3913	237	10.1	116	18.3
3913	237	10.3	105	16.5
3913	237	11.7	137	21.6
4843	293	10.0	118	20
4843	293	9.67	81.2	13.7
4843	293	10.3	123	20.8
1215[a]	24.5[a]	76.3[a]	305[a]	32.5[a]

[a] Three cells within canister.

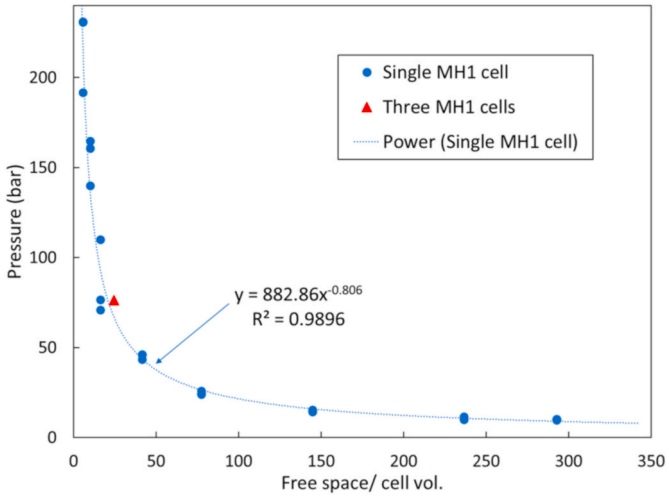

Fig. 6. A plot of an inverse power relationship between MH1 cell TR pressure and the ratio of free space-to-cell volume.

test with 685 mL of free space. A small amount of gas was generated during cell venting prior to TR. A much larger amount was generated during TR. The plot of ambient gas volume varies significantly at TR, attributed in part to differences in temperature and pressure sampling rates between the two data acquisition systems. Also, it takes some time after TR for the gas temperature to approach uniformity for ideal gas law calculation purposes (Koch et al., 2018; Hoelle et al., 2021). Ambient gas volume calculations became stable about 1 min after TR. The average and range of ambient volumes for sixteen MH1 ARC tests calculated 1 min after TR are summarized in Table 3. Gas volumes generated per cell capacity and per cell energy are also included. The gas volumes per cell capacity are within the range of those reported by Koch et al. (2018) and Hoelle et al. (2021).

Researchers observed that the quantity of gas produced by the MH1 cells tended to increase with canister volume as shown in Fig. 13. This

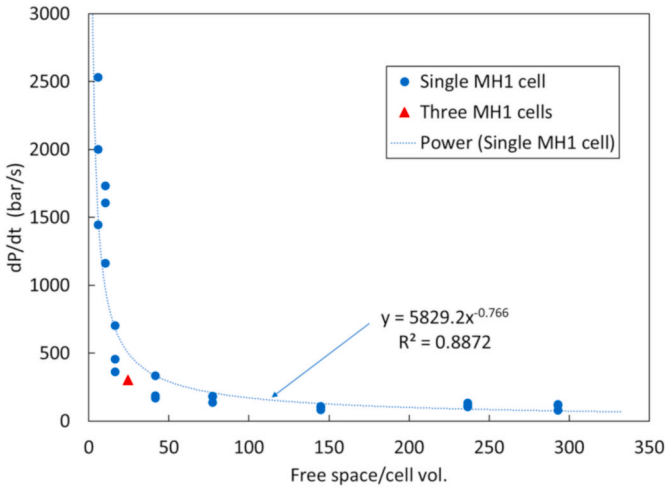

Fig. 7. A plot of an inverse power relationship between MH1 cell maximum TR pressure rise rate and the ratio of free space-to-cell volume.

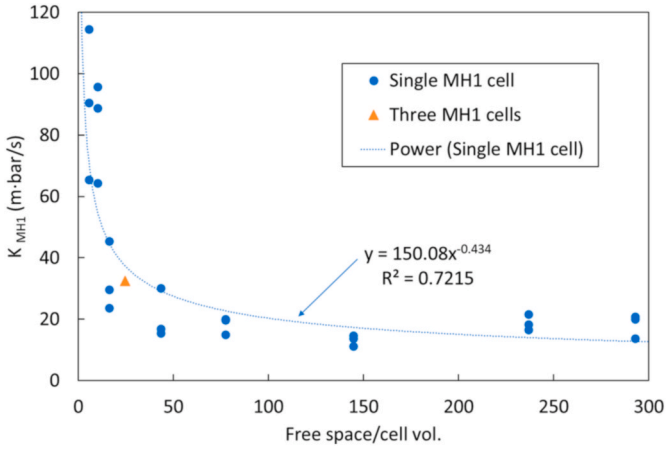

Fig. 8. A plot of an inverse power relationship between K_{MH1} and the ratio of free space-to-cell volume.

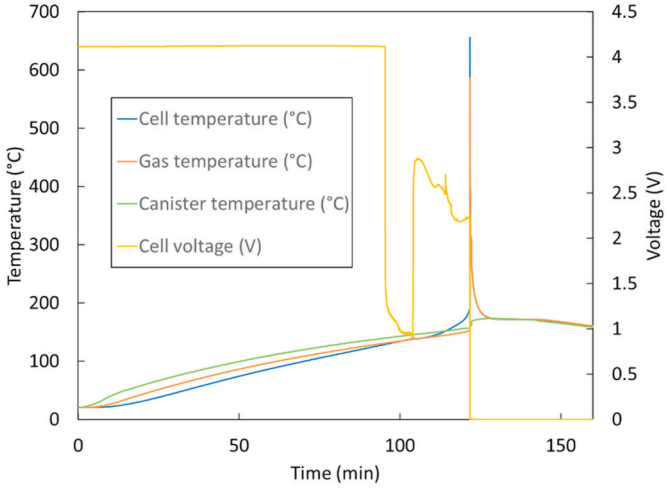

Fig. 9. Time plots of temperatures and voltage for an MH1 cell with 685 mL free space.

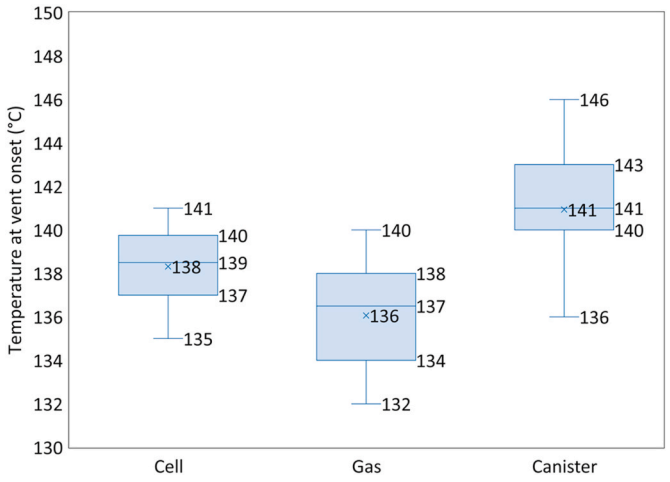

Fig. 10. Box and whisker plots summarizing MH1 cell, gas, and canister temperatures at venting onset.

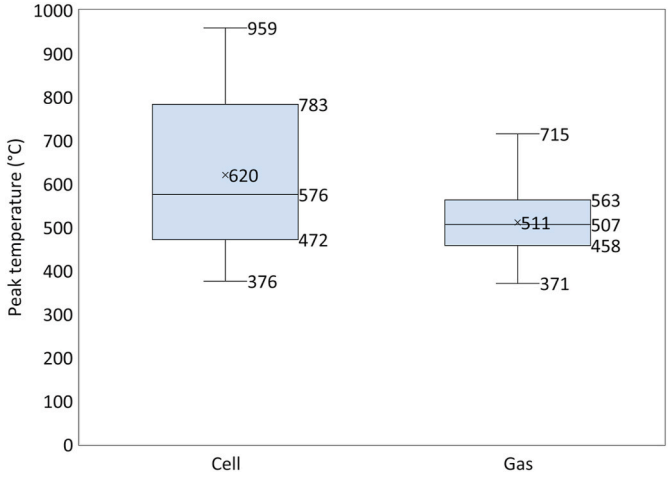

Fig. 11. Box and whisker plots summarizing peak MH1 cell and gas temperatures.

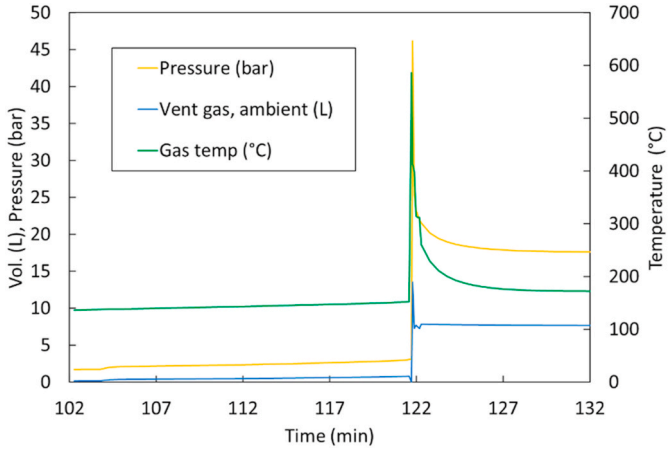

Fig. 12. Vent gas volume at ambient conditions calculated from pressure and gas temperature (685 mL of free space).

Table 3
Quantities of gas produced by the MH1 cells 1 min after thermal runaway (16 tests).

	Moles	Gas vol. (L)	Gas vol./capacity (L/Ah)	Gas vol./energy (L/Wh)
Average	0.42	7.6	2.4	0.66
Range	0.3 to 0.54	6.8 to 8.3	2.1 to 2.6	0.58 to 0.71

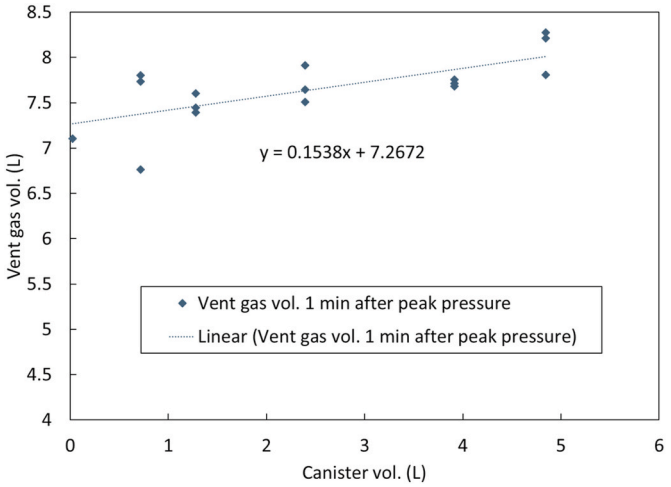

Fig. 13. Vent gas production tended to increase with canister volume.

trend is consistent with Le Chatelier's principle regarding the effect of change in volume. With a pressure decrease due to an increase in volume, the side of the chemical reaction equilibrium with more moles is favored.

3.4. NMC pouch cell ARC test

Fig. 14 shows time plots and Table 4 provides summary data for the 100-Ah NMC pouch cell ARC test. The cell thermocouple was inserted between the pouch foil and enclosure wall after the cell was inserted in the enclosure. The thermocouple tip was likely in contact with the pouch-cell foil and the internal wall of this form-fitting enclosure. The vent-gas thermocouple was placed by the enclosure pressure relief valve vent (Fig. 2). The enclosure thermocouple was taped to the enclosure exterior. A video camera was positioned to view the pressure relief valve

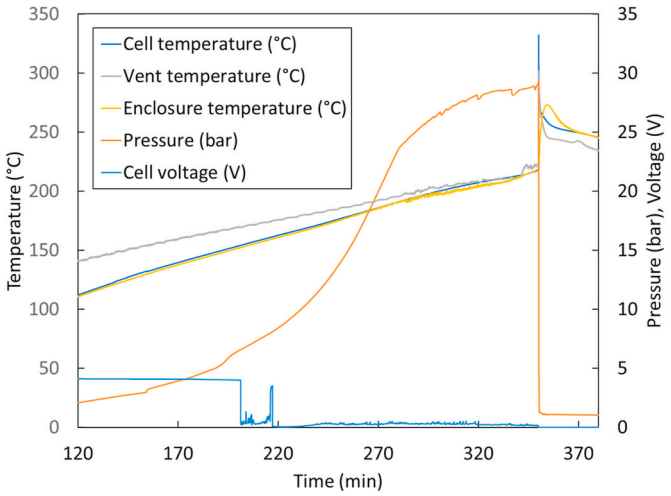

Fig. 14. Time plots for the 100-Ah NMC pouch ARC test.

Table 4
Summary data for the 100-Ah NMC pouch ARC test.

Pressure relief valve activation (bar)	29.4 (426 psia)
Cell peak temperature (°C)	332
TR onset temperature (°C)	218
Vent gas peak temperature (°C)	302
Enclosure peak temperature (°C)	273

mounted in the enclosure wall. The enclosure seals were checked prior to the ARC test by pressurizing the enclosure to 11.5 bar using a hand pump. TR onset began when the cell temperature reached approximately 218 °C. The cell temperature reached 332 °C during TR and the enclosure temperature reached 273 °C a few minutes after TR. The cell and enclosure temperatures tracked closely together prior to TR (Fig. 14). Heat sinking to the enclosure wall in contact with the pouch cell and thermocouple likely reduced the cell temperature measurement during TR. The video showed that smoke was released through the enclosure pressure relief valve during TR. The pressure reached 29.4-bar before the pressure was relieved abruptly. Pressure dips occurring before the abrupt pressure drop indicate gas escaping the enclosure. The enclosure was pressurized to 2 bars after the test, and significant leaks were found around the rubber gaskets. The pressure dips and overall gradual reduction in pressure rise rate prior to TR were evidently due to gas escaping through the rubber gaskets and pressure relief valve. Even with these apparent leaks, the test confirmed that the TR pressure of this cell exceeded the 8.62-barg (125-psig) pressure generation threshold for conventional MSHA-approved XP enclosures (MSHA, 2005) by a significant margin.

4. Discussion

The MH1 cell TR pressures are significantly higher than the LFP cell TR pressures studied previously (Dubaniewicz et al., 2021), under comparable confinement conditions. Fig. 15 shows the highest pressure per cell-canister combination for the MH1 and LFP cells. The 9.62-bar (absolute) threshold corresponds to the 125-psig specification for conventional MSHA-approved XP enclosures. Using the maximum MH1 cell TR pressure curve fit equation shown in Fig. 15, approximately 287 times the MH1 cell volume of free space would be needed to meet the 125-psig specification. This compares to approximately 34 times the LFP cell volume to meet the same threshold (Dubaniewicz et al., 2021). Where battery enclosure internal volume restrictions may prevent adequate free space, TR cascade prevention and venting with properly designed and maintained flame arrestors are potential mitigation strategies for excessive overpressures (Dubaniewicz et al., 2021). Criteria for evaluation and testing of MSHA-approved XP enclosures may need to consider the cumulative internal pressure resulting from a simultaneous CH_4-air ignition and the pressure for a TR event from a Li-ion cell.

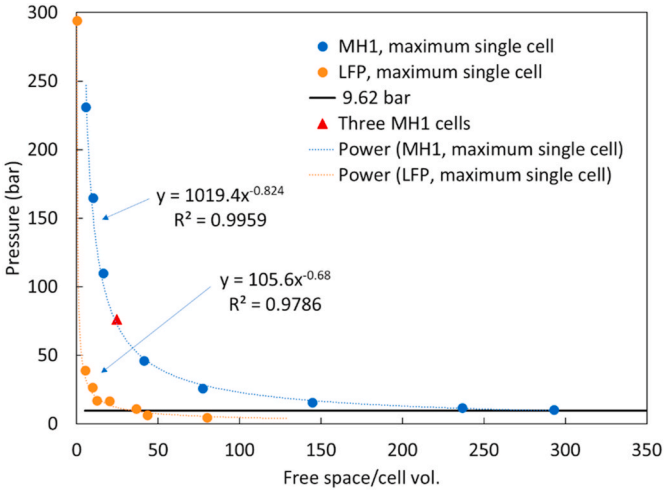

Fig. 15. Comparison of maximum TR pressures of MH1 and LFP cells in relation to the 9.62 bar threshold for conventional MSHA-approved XP enclosures.

K values for gas-air deflagrations may tend to increase with vessel volume (Cashdollar et al., 2000). Fig. 8 shows a different trend for the MH1 cell TR where K_{MH1} values increase with decreasing volume. This volume dependency should be taken into consideration for deflagration vents designed for battery enclosures, particularly for those that provide relatively little free space around Li-ion batteries.

The trends for the MH1 cell TR (Figs. 6–7) indicate that smaller free spaces than studied here may produce significantly larger pressures and pressure rise rates. Further testing with form-fitting enclosures with little free space would better characterize maximum potential pressures and pressure rise rates within cell casings of cells subjected to TR.

Dubaniewicz et al. (2021) reviewed CH_4-air and coal dust ignition temperatures for the explosion hazard in gassy underground mines and underground coal mines. Referring to Figs. 10–11, after subtracting temperature rise due to ARC heating, the MH1 cell TR can reach temperatures exceeding the CH_4-air autoignition temperature (600 °C observed) and coal dust layer and coal dust cloud ignition temperatures by several hundred °C. In contrast, the TR temperatures of LFP cells were below the autoignition temperature of CH_4-air (Dubaniewicz et al., 2021). TR of an MH1 cell should be considered as a potential ignition source for CH_4-air mixtures, coal dust layers, and coal dust clouds in gassy underground mines and underground coal mines. Because atmospheric oxygen is not required to sustain TR, TR may continue for an extended period of time within an XP Li-ion battery enclosure, creating a potential for excessive enclosure surface temperature. Along with ambient CH_4, vented Li-ion cell gases mixed with air may form flammable gas-air mixtures, which may be ignited by a sufficiently strong ignition source such as an electrical fault of a large-format battery. These secondary explosion or fire hazards are distinct from TR in that they involve atmospheric oxygen.

Dubaniewicz et al. (2021) reported that a 26650 LFP cell TR produced about 4.35 L of gas (ambient), corresponding to 1.14 L/Ah or 0.36 L/Wh. The MH1 cells with a similar energy produced significantly larger amounts of gas (Table 3). The larger gas amounts and higher temperatures associated with the MH1 cell TR account for the higher pressures observed in this study.

The MH1 cells were tested at a full state of charge. The severity of the TR increases with an increasing state of charge (Golubkov et al., 2015). Liu et al. (2021) found evidence of thermite reactions involving aluminum cell components under overcharge conditions. Results of this study should not be considered conservative for cells at an excessive state of charge due to overcharge.

Differences in cell additives can influence failure response (Baird et al., 2020). NMC cathode cells with different formulations or additives may produce different results than reported here.

5. Conclusions

NIOSH PMRD researchers are developing workplace solutions to reduce explosion risks of Li-ion batteries in mining equipment.

Inverse power relationships were observed with the amount of free space for NMC cathode model MH1 18650 Li-ion cell thermal runaway pressures and pressure rise rates. A confined MH1 cell with 92.5 mL of free space produced 232 bar of pressure, far exceeding minimum pressure containment specifications for conventional MSHA-approved explosion-proof enclosures. Significantly higher pressures and pressure rise rates should be expected with lower amounts of free space. A curve fit to the data indicates that approximately 287 times the MH1 cell volume of free space would be needed to meet the 8.62-barg (125-psig) MSHA pressure generation threshold specification. The MH1 cell thermal runaway pressures were significantly higher than those for LFP cells

with similar energies studied previously, under comparable confinement conditions.

Deflagration index values for MH1 cell thermal runaway increased with decreasing canister volume, in contrast to values for gas-air deflagrations that may decrease with decreasing volumes. This should be taken into consideration for deflagration vents designed for Li-ion battery enclosures, particularly for those that provide relatively little free space around Li-ion batteries.

The MH1 cell thermal runaway can reach temperatures exceeding the CH_4-air autoignition temperature (600 °C observed) and coal dust layer and coal dust cloud ignition temperatures. Thermal runaway of MH1 cells should be considered as a potential ignition source for CH_4-air mixtures, coal dust layers, and coal dust clouds in gassy underground mines and underground coal mines.

The quantity of gas produced by the MH1 cells tended to increase with canister volume, consistent with Le Chatelier's principle regarding the effect of change in volume. The highest gas production was 0.71 L/Wh for one cell. Gas evolved per cell energy (L/Wh) should be used rather than per current capacity (L/Ah) when scaling up gas production from a failing cell to electrical ratings for a large-format battery with series connected cells.

Disclaimer

The findings and conclusions in this report are those of the authors and do not necessarily represent the official position of the National Institute for Occupational Safety and Health, Centers for Disease Control and Prevention. Mention of any company or product does not constitute endorsement by NIOSH.

Author contribution

Thomas H. Dubaniewicz: Conceptualization, Methodology, Formal analysis, Investigation, Writing - Original Draft, Visualization, Project administration, Teresa L. Barone: Methodology, Formal analysis, Investigation, Writing - Original Draft, Connor B. Brown: Investigation, Formal analysis, Richard A. Thomas: Investigation.

Declaration of competing interest

The authors declare that they have no known competing financial interests or personal relationships that could have appeared to influence the work reported in this paper.

References

Adams, R.A., Mistry, A.N., Mukherjee, P.P., Pol, V.G., 2019. Materials by design: tailored morphology and structures of carbon anodes for enhanced battery safety. ACS Appl. Mater. Interfaces 11, 13334–13342. https://doi.org/10.1021/acsami.9b02921.

Baird, A.R., Archibald, E.J., Marr, K.C., Ezekoye, O.A., 2020. Explosion hazards from lithium-ion battery vent gas. J. Power Sources 446, 227257.

Campion, C.L., Li, W., Euler, W.B., Lucht, B.L., Ravdel, B., DiCarlo, J.F., Gitzendanner, R., Abraham, K.M., 2004. Suppression of toxic compounds produced in the decomposition of lithium-ion battery electrolytes. Electrochem. Solid State Lett. 7, A194. https://doi.org/10.1149/1.1738551.

Cashdollar, K.L., Zlochower, I.A., Green, G.M., Thomas, R.A., Hertzberg, M., 2000. Flammability of methane, propane, and hydrogen gases. J. Loss Prev. Process. Ind. 13, 327–340.

Dubaniewicz Jr., T.H., DuCarme, J.P., 2016. Internal short circuit and accelerated rate calorimetry tests of lithium-ion cells: considerations for methane-air intrinsic safety and explosion proof/flameproof protection methods. J. Loss Prev. Process. Ind. 43, 575–584. https://www.ncbi.nlm.nih.gov/pmc/articles/PMC5040472/.

Dubaniewicz, T.H., Zlochower, I., Barone, T., Thomas, R., Yuan, L., 2021. Thermal runaway pressures of iron phosphate lithium-ion cells as a function of free space within sealed enclosures. Mining, Metallurgy & Exploration 38, 539–547. https://doi.org/10.1007/s42461-020-00349-9.

Duh, Y.-S., Tsai, M.-T., Kao, C.-S., 2017. Thermal runaway on 18650 lithium-ion batteries containing cathode materials with and without the coating of self-terminated oligomers with hyper-branched architecture (STOBA) used in electric vehicles. J. Therm. Anal. Calorim. 129, 1935–1948.

Duh, Y.-S., Sun, Y., Lin, X., Zheng, J., Wang, M., Wang, Y., Lin, X., Jiang, X., Zheng, Z., Zheng, S., Yu, G., 2021. Characterization on thermal runaway of commercial 18650 lithium-ion batteries used in electric vehicles: a review. J. Energy Storage 41, 102888. https://doi.org/10.1016/j.est.2021.102888.

Finegan, D.P., Darcy, E., Keyser, M., Tjaden, B., Heenan, T.M.M., Jervis, R., Bailey, J.J., Vo, N.T., Magdysyuk, O.V., Drakopolous, M., Di Michiel, M., Rack, A., Hinds, G., Brett, D.J.L., Shearing, P.R., 2018. Identifying the cause of rupture of Li-ion batteries during thermal runaway. Adv. Sci. 5, 1700369. 13.

Gillett, S., 2021. Battery Electric Vehicle Emergency Response Incident Review and Best Practices. Workplace Safety North Virtual Symposium: Battery Electric Vehicle Safety in Mines, January 20, 2021. Retrieved August 2021 from. https://www.workplacesafetynorth.ca/resources/virtual-symposium-battery-electric-vehicle-safety-mines.

GMG, 2018. Recommended Best Practices for Battery Electric Vehicles in Underground Mining –. Global Mining Guidelines Group Document No.: 20180621_UG_Mining_BEV-GMG-WG-v02-r01. Retrieved August 2021 from, second ed.. https://gmggroup.org/guidelines/.

Golubkov, A.W., Scheikl, S., Planteu, R., Voitic, G., Wiltsche, H., Stangl, C., Fauler, G., Thaler, A., Hacker, V., 2015. Thermal runaway of commercial 18650 Li-ion batteries with LFP and NCA cathodes – impact of state of charge and overcharge. RSC Adv. 5, 57171–57186.

Gully, B., Helgesen, H., Skogtvedt, J.E., Kostopoulos, D., 2019. Technical Reference for Li-Ion Battery Explosion Risk and Fire Suppression. DNV GL Report No.: 2019-1025, Rev. 4. 202 pp. Retrieved August 2021 from. https://www.dma.dk/Documents/Publikationer/TechnicalReferenceLi-ionBatteryExplosionRiskFireSuppression.pdf.

Harris, S.J., Timmons, A., Pitz, W.J., 2009. A combustion chemistry analysis of carbonate solvents used in Li-ion batteries. J. Power Sources 193, 855–858. https://doi.org/10.1016/j.jpowsour.2009.04.030.

Henriksen, M., Vaagsaether, K., Lundberg, J., Forseth, S., Bjerketvedt, D., 2019. Explosion characteristics for Li-ion battery electrolytes at elevated temperatures. J. Hazard Mater. 371, 1–7.

Hill, D., 2020. McMicken Battery Energy Storage System Event Technical Analysis and Recommendations. DNV GL Document No.: 10209302-HOU-R-01, July 18, 2020, p. 70.

Hoelle, S., Scharner, S., Asanin, S., Hinrichsen, O., 2021. Analysis on thermal runaway behavior of prismatic lithium-Ion batteries with autoclave calorimetry. J. Electrochem. Soc. 168, 120515.

Jacques, D., 2019. BEV Pioneering Partnership at Borden—Celebrate the Wins, Face the Challenges. Mining Diesel Emissions Council. MDEC 2019, October 7-10, Toronto, ON. S6P3. Retrieved August 2021 from. https://mdec.ca/2019/S6P3_David_Jacques.pdf.

Jhu, C.-Y., Wang, Y.-W., Wen, C.-Y., Shu, C.-M., 2012. Thermal runaway potential of $LiCoO_2$ and $Li(Ni_{1/3}Co_{1/3}Mn_{1/3})O_2$ batteries determined with adiabatic calorimetry methodology. Appl. Energy 100, 127–131.

Koch, S., Fill, A., Birke, K.P., 2018. Comprehensive gas analysis on large scale automotive lithium-ion cells in thermal runaway. J. Power Sources 398, 106–112.

Kurpiel, W., Deja, P., Polnik, B., Skora, M., Miedzinski, B., Habrych, M., Debita, H., Zamlynska, M., Falkowski-Gilski, P., 2021. Performance of passive and active balancing systems of lithium batteries in onerous mine environment. Energies 14, 7624.

Leonida, C., 2021. BEV technology: what's next? Eng. Min. J. 222 (1), 40–44. Retrieved August 2021 from. https://www.e-mj.com/features/bev-technology-whats-next/.

Liu, W., Zhao, F., Liu, S., Mi, W., 2021. Chemical analysis of the cause of thermal runaway of lithium-ion iron phosphate batteries. J. Electrochem. Soc. 168, 060507.

McKinnon, M.B., DeCrane, S., Kerber, S., 2020. Four Firefighters Injured in Lithium-Ion Battery Energy Storage System Explosion – Arizona. July 28, 2020. UL Firefighter Safety Research Institute, Columbia, MD, p. 58.

Mishra, D., Shah, K., Jain, A., 2021. Investigation of the impact of flow of vented gas on propagation of thermal runaway in a Li-ion battery pack. J. Electrochem. Soc. 168, 060555.

MSHA, 2005. Requirements for Explosion Testing Per 30 CFR, 18.62. ASTP 2137. U.S. Department of Labor, Mine Safety and Health Administration, Arlington, VA, USA. Retrieved August 2021 from. https://arlweb.msha.gov/techsupp/acc/standardtestprocs/ASTP2137.pdf.

Nestler, T., Schmid, R., Münchgesang, W., Bazhenov, V., Schilm, J., Leisegang, T., Meyer, D.C., 2014. Separators-technology review: ceramic based separators for secondary batteries. AIP Conf. Proc. 1597, 155–184. https://doi.org/10.1063/1.4878486.

NFPA, 2018. NFPA 68, Standard on Explosion Protection by Deflagration Venting. National Fire Protection Association, Quincy, MA, p. 100.

NIOSH, 2020. Mining Project: Advanced Strategies for Controlling Exposures to Diesel Aerosols. U.S. Department of Health and Human Services, Centers for Disease Control and Prevention, National Institute for Occupational Safety and Health. Retrieved August 2021 from. https://www.cdc.gov/niosh/mining/researchprogram/projects/project_DieselAerosols.html.

Nitta, N., Wu, F., Lee, J.T., Yushin, G., 2015. Li-ion battery materials: present and future. Mater. Today 18, 252–264. https://doi.org/10.1016/j.mattod.2014.10.040.

Park, Y.S., Lee, S.M., 2009. Effects of particle size on the thermal stability of lithiated graphite anode. Electrochim. Acta 54, 3339–3343. https://doi.org/10.1016/j.electacta.2008.12.030.

Pyroban, 2021. Confused about "ATEX" compliant lithium-ion forklift Batteries? Retrieved August 2021 from. https://www.pyroban.com/confused-about-atex-compliant-lithium-ion-forklift-batteries/.

Raja, M., Sanjeev, G., Kumar, T.P., Stephan, A.M., 2015. Lithium aluminate-based ceramic membranes as separators for lithium-ion batteries. Ceram 41, 3045–3050. https://doi.org/10.1016/j.ceramint.2014.10.142.

Stephens, D., Shawcross, P., Stout, G., Sullivan, E., Saunders, J., Risser, S., Sayre, J., 2017. Lithium-ion Battery Safety Issues for Electric and Plug-In Hybrid Vehicles

(Report No. DOT HS 812 418). National Highway Traffic Safety Administration, Washington, DC. Retrieved August 2019 from. https://www.nhtsa.gov/sites/nhtsa.dot.gov/files/documents/12848-lithiumionsafetyhybrids_101217-v3-tag.pdf.

U.S. Code of Federal Regulations, 2021. Title 30, Part 18, Section 18.23 Limitation of external surface temperatures and Section 18.62 Tests to determine explosion-proof characteristics. Retrieved August 2021 from. https://ecfr.federalregister.gov/current/title-30.

Yao, X.-Y., Kong, L., Pecht, M.G., 2020. Reliability of cylindrical Li-ion battery safety vents. IEEE Access 8, 101859–101866. Retrieved August 2021 from. https://ieeexplore.ieee.org/stamp/stamp.jsp?arnumber=9099837.

Yayathi, S., Walker, W., Doughty, D., Ardebili, H., 2016. Energy distributions exhibited during thermal runaway of commercial lithium ion batteries used for human spaceflight applications. J. Power Sources 329, 197–206.

Yuan, L., Dubaniewicz, T.H., Zlochower, I., Thomas, R., Rayyan, N., 2020. Experimental study on thermal runaway and vented gases of lithium-ion cells. Process Saf. Environ. Protect. 144, 186–192.

Zalosh, R., Gandhi, P., Barowy, A., 2021. Lithium-ion energy storage battery explosion incidents. J. Loss Prev. Process. Ind. 72, 104560. https://doi.org/10.1016/j.jlp.2021.104560.

Zhao, C., Sun, J., Wang, Q., 2020. Thermal runaway hazards investigation on 18650 lithium-ion battery using extended volume accelerating rate calorimeter. J. Energy Storage 28, 101232.